electronics

Article

Enhancing Artifact Protection in Smart Transportation Monitoring Systems via a Porous Structural Triboelectric Nanogenerator

Jiabin Zhang [1,2,†], Erming Su [1,2,†], Chengyu Li [2,3,†], Shuxing Xu [1,2], Wei Tang [1,2,3], Leo N.Y. Cao [2,3], Ding Li [1,2,3,*] and Zhong Lin Wang [2,3,4,*]

1 Center on Nanoenergy Research, School of Physical Science and Technology, Guangxi University, Nanning 530004, China; zhangjiabin@binn.cas.cn (J.Z.); suerming@binn.cas.cn (E.S.); xushuxing@binn.cas.cn (S.X.); tangwei@binn.cas.cn (W.T.)
2 Beijing Key Laboratory of Micro-Nano Energy and Sensor, Beijing Institute of Nanoenergy and Nanosystems, Chinese Academy of Sciences, Beijing 101400, China; lichengyu@binn.cas.cn (C.L.); caonanying@binn.cas.cn (L.N.Y.C.)
3 School of Nanoscience and Engineering, University of Chinese Academy of Sciences, Beijing 100049, China
4 School of Materials Science and Engineering, Georgia Institute of Technology, Atlanta, GA 30332-0245, USA
* Correspondence: liding@binn.cas.cn (D.L.); zhong.wang@mse.gatech.edu (Z.L.W.)
† These authors contributed equally to this work.

Abstract: Artifacts are irreplaceable treasures of human culture, and transportation monitoring is critical for safeguarding valuable artifacts against damage during culture exchanges. However, current collision-monitoring technologies have limitations in regard to real-time monitoring, cushioning protection, and power supply requirements. Here, we present a method for constructing a smart artifact-monitoring system (SAMS) based on a porous carbon black (CB)/Ecoflex triboelectric nanogenerator (PCE-TENG) that can monitor collisions in real time and absorb vibrations during artifact transportation. The PCE-TENG is assembled using a flexible printed circuit board (FPCB) and a porous Ecoflex layer with CB powder. It exhibits cushioning protection, stretchability, pressure sensitivity, and durability. To enhance its electrical output, modifications were made to optimize the CB content and surface structure. The SAMS comprises six PCE-TENGs attached to the inner wall of the artifact transport package and enables collision monitoring and protection in different directions. Moreover, the SAMS has the capability to instantly transmit warning information to monitoring terminals in the event of improper operations, empowering carriers to promptly and efficiently safeguard artifacts by taking necessary measures. This paper presents a practical strategy for artifact transportation monitoring and package engineering that could have significant implications for the field.

Keywords: artifact transportation; collision monitoring; vibration absorption; self-powered; triboelectric nanogenerator

Citation: Zhang, J.; Su, E.; Li, C.; Xu, S.; Tang, W.; Cao, L.N.Y.; Li, D.; Wang, Z.L. Enhancing Artifact Protection in Smart Transportation Monitoring Systems via a Porous Structural Triboelectric Nanogenerator. *Electronics* **2023**, *12*, 3031. https://doi.org/10.3390/electronics12143031

Academic Editor: Dung-An Wang

Received: 2 June 2023
Revised: 24 June 2023
Accepted: 26 June 2023
Published: 10 July 2023

1. Introduction

Artifacts are irreplaceable treasures of human culture that embody the splendid civilization of humankind [1–3]. With the increasing demand for exchange and mutual learning among different nations, artifact exchanges between museums have become more frequent. This has naturally led to an increase in artifact transportation [4], and the monitoring and protection of artifacts during transportation are particularly important considering their preciousness, fragility, and irreplaceable nature [5,6]. Collision monitoring is among the most essential aspects of transportation monitoring, playing an important role in protecting fragile artifacts from damage by impacts and vibrations during transportation [7–9]. At present, shock indicator labels are widely used to provide visual warnings and determine whether a collision has occurred during transportation [10], but they are one-time indications and do not allow for real-time monitoring. Acceleration sensors could provide continuous monitoring of the status of the overall package [4,11], though they are unable to detect specific pressures on the artifacts inside the package, which is more important for artifact protection. In addition, they are not intended for use as vibration absorbers due to their rigid configurations, and they need an external power supply.

Compared with traditional sensors, triboelectric nanogenerators (TENGs) operate without the need for an external power source, thus making them suitable as self-powered sensors that can detect vibrations [12–16], acceleration [17–20], fluid [21–24], and pressure [25–27]. For example, Rana et al. developed a self-powered switch using PVDF-TrFE/MXene nanofibers to control electrical home appliances [28]. Since the TENG was first invented in 2012 [29], it has been proven to effectively convert low-frequency, irregular, and distributed mechanical energy into electrical energy by coupling contact electrification and electrostatic induction [20–32]. The advantages of TENGs include their easy fabrication, cost-effectiveness, and the abundant materials and structural choices that can be employed. Some studies have explored the use of TENGs as sensors for monitoring impacts and collisions. For instance, Heo et al. developed a self-powered impact sensor to detect an external impact's magnitude and direction [33]. Liu et al. used a grating-structured free-standing TENG as an acceleration sensor for self-powered real-time collision detection [34]. However, the above sensors do not have a cushioning function and are unsuitable for artifact transportation. Kou et al. developed an array of TENG pressure sensors based on porous PDMS with a cushion function [35], but its electrode structure was fixed and thus unsuitable for building a monitoring system for artifacts of various shapes. Thus, the development of a smart monitoring system for artifact transportation utilizing TENG pressure sensors with a cushioning function and flexible electrode structure is necessary.

Here, we report a smart artifact-monitoring system (SAMS) for vibration absorption and collision monitoring in real time during artifact transportation. It consists of an easily fabricated and self-powered porous carbon black (CB)/Ecoflex triboelectric nanogenerator (PCE-TENG) sensor with a cushion function, multi-channel wireless data acquisition, a processing and transmission circuit board, and a monitoring terminal. The PCE-TENG is assembled using porous CB/Ecoflex and a serpentine-structured flexible printed circuit board (FPCB) to obtain excellent stretchability. Its porous structure is obtained using a simple and low-cost sacrificial template method (CB particles are embedded in an Ecoflex matrix and manufactured using the citric acid monohydrate (CAM) sacrificial template method). The electrical output of the PCE-TENG can be enhanced by modifying the CB powder content and adjusting the CAM/Ecoflex mixing ratio. The optimized PCE-TENG has cushioning properties, pressure sensitivity, and excellent stability. A SAMS is attached to the artifact transport package to achieve collision monitoring and protection against collisions from different directions. Six PCE-TENGs are attached and function as pressure sensors that monitor the pressure of the six inner faces of the artifact transport package. The integrated circuit board can collect and transmit collision signals to the monitoring terminal in real time via Wi-Fi, thus avoiding a messy arrangement of wires. A LabVIEW real-time alarm program is developed to acquire and process the signals from the Wi-Fi module, and this helps carriers to accurately judge the position of the artifact via an alarm mechanism. The SAMS offers a novel method for monitoring and safeguarding artifacts during transportation; it has potential applications in various fields related to the packaging and transportation of fragile objects.

2. Experimental Section

2.1. Fabrication of the Porous CB/Ecoflex TENG

The fabrication procedure of the porous CB/Ecoflex is shown in Figure 1b. Firstly, a mixture of silicone rubber (Ecoflex 00-30, Smooth-on) base and curing agent was prepared with a weight ratio of 1:1. Then, CB powder at various mass ratios (0 wt%, 1 wt%, 2 wt%, 3 wt%, 5 wt%, 7 wt%, and 10 wt%) was added to the prepared Ecoflex mixture in a sequential manner; the mixing ratios of CAM and Ecoflex were controlled by adjusting the mass ratio between the CAM particles and the Ecoflex mixture. After thorough mixing and stirring, the resulting mixture was transferred into a pre-made acrylic mold of a specific size (70 × 70 × 5 mm^3). The mold containing the mixture was placed in a vacuum dryer to completely remove air bubbles, then cured in an oven at 60 °C for 4 h. Subsequently, the solidified sample was precisely cut to dimensions of 2 × 2 cm^2 and submerged in ethanol until the CAM particles were completely removed from the mixture. Notably, no additional heating or ultrasound treatment was necessary for this template removal process [36,37]. Finally, the soaked sample was dried in an oven at 60 °C for 4 h, and porous CB/Ecoflex was obtained.

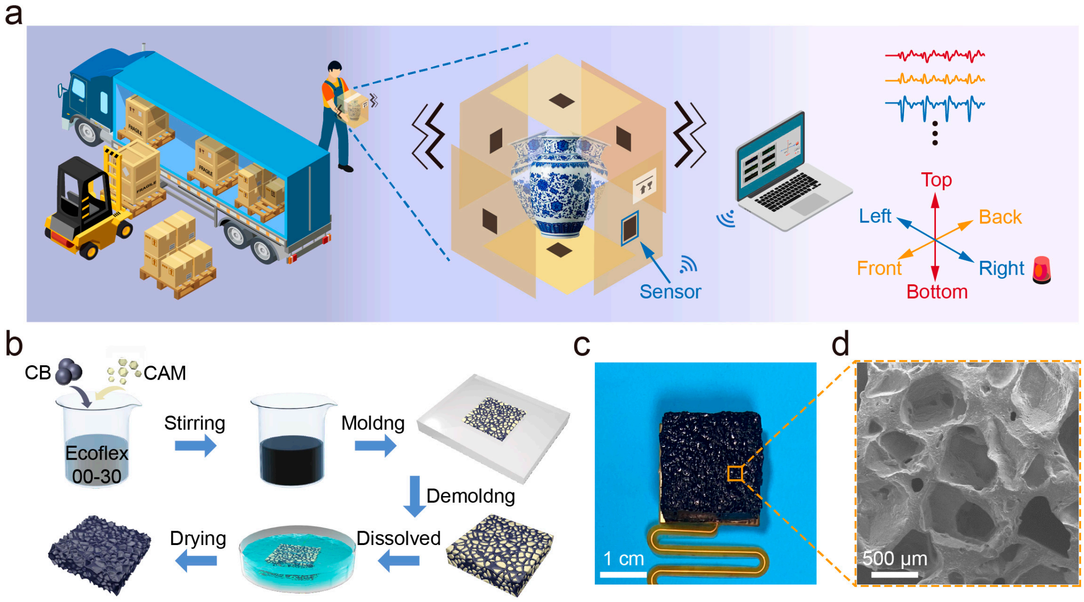

Figure 1. The concept and fabrication of the smart artifact-monitoring system (SAMS) based on porous carbon black (CB)/Ecoflex triboelectric nanogenerators (PCE-TENGs). (**a**) A potential application scenario of the SAMS during artifact transportation. PCE-TENGs are attached to the inner wall of the artifact transport box to absorb shocks and collect vibration signals. The collected signals are transmitted to monitoring terminals through Wi-Fi communication in real time, with alert feedback provided to the carrier when the vibration pressure is over the pre-set level. (**b**) Schematic diagram of the fabrication process of porous CB/Ecoflex. (**c**) Photograph of a PCE-TENG consisting of porous CB/Ecoflex and the FPCB. (**d**) SEM image of the porous CB/Ecoflex.

Double-sided PI tape was purchased directly from merchants. The copper on the surface of the FPCB was prepared by a copper-plating process. The porous CB/Ecoflex was securely attached to the Cu electrode using the double-sided PI tape to create a PCE-TENG.

2.2. Characterization and Measurement

The morphology in micro-scale of the porous CB/Ecoflex was characterized by using a cold-field-emission electron microscope (SU8020, Hitachi, Tokyo, Japan) to obtain SEM images. A LinMot E1100 linear motor was utilized to generate the cyclic contact-separation motion for the PCE-TENG. In the experiment, the frequency of the linear motor was 0.5–3 Hz, and the amplitude was 6 cm. The output signals (Voc, Isc, and Qsc) were measured using a Keithley 6514 system electrometer. Images of the overall view of the porous CB/Ecoflex were acquired through micro-CT (Quantum GX, PerkinElmer, Waltham, MA, USA). The rebound height of the steel ball after hitting the sample was recorded using a high-speed camera (FASTCAM Mini AX, Photron, Tokyo, Japan). The falling height of the steel ball was 25 cm, and the mass of the steel ball was 100 g. The voltage measurement of the PCE-TENG in the SAMS primarily utilized a specifically designed wireless multi-channel acquisition circuit comprising a power management integrated circuit (PMIC), a 16-bit analog–digital (AD) converter module (AD7606), a pre-charge amplifier, a wireless communication module (ESP32), and a main control chip (STM32L431). The TENG signal was amplified by the front-end amplifier and then digitized by the AD chip. The signal was subsequently transmitted to the monitoring terminal through a Wi-Fi module, which was controlled by the master control chip (6 signal channels with each channel having a data sampling rate of 2 $K \cdot s^{-1}$). The monitoring terminals received, displayed, and stored the data using a LabVIEW computer program for further analysis and decision making. (The details of the circuit diagram are depicted in Figure S1, Supplementary Materials.)

3. Results and Discussion

3.1. Fabrication of the PCE-TENG and Its Characterization

Figure 1a shows a potential application scenario of the SAMS. The system comprises six PCE-TENGs; an integrated circuit board with functions of multi-channel signal acquisition, processing, and Wi-Fi transmission; and a monitoring terminal with a LabVIEW real-time alarm program. The six PCE-TENGs are placed at the six inner faces of the artifact transport package as self-powered pressure sensors to monitor collisions from different directions and absorb vibrations. When vibrations or impacts occur during the transportation of artifacts, the PCE-TENGs can not only detect the collision magnitude and direction in real time but also provide extra cushioning for artifacts against the collision force from outside. Moreover, based on the voltage signals received by wireless transmission, the SAMS will issue an alarm when the collision level surpasses the pre-set threshold and provide real-time visual feedback. This reminds the truck driver or the worker to lower their speed or pay attention to their carrying actions to better protect the artifact. This reveals the potential of the SAMS for artifact transportation monitoring and protection within the context of emerging technologies such as the Internet of Things (IoT), blockchain, big data, and artificial intelligence.

Figure 1b illustrates a schematic diagram outlining the fabrication processes involved in creating the porous CB/Ecoflex. CB powder and CAM particles were combined with the Ecoflex00-30 pre-polymer. Following stirring, molding, demolding, and curing, the CAM particles in the mixture were dissolved in ethanol. Finally, the dried porous CB/Ecoflex structure was assembled with an FPCB to make a PCE-TENG (Figure 1c). The morphology of the porous CB/Ecoflex in micro-scale was visualized through scanning electron microscopy (SEM) (Figure 1d). The porous structure makes it compressible and recoverable (Figure S2, Supplementary Materials).

These properties of the PCE-TENG enable the SAMS to be more effective and safer, ultimately minimizing the detrimental effects of collisions on the artifacts. The SAMS will thus provide a new strategy for artifact transport monitoring and conservation.

3.2. Working Principle and Fundamental Characteristics of the PCE-TENG

To demonstrate the unique properties of the PCE-TENG, we set up an experimental platform, as shown in Figure 2a, including a linear motor and an ergometer. Before each test, we calibrated the pressure required for the test by fine-tuning the micrometer. The PCE-TENG fixed onto the ergometer was periodically placed in contact with the polyimide (PI) film. The PI film served as a movable dielectric material that was controlled by the linear motor at a given frequency. The PCE-TENG is a single-electrode model TENG, and its structure is shown in Figure 2b. The uppermost layer is porous CB/Ecoflex as a contact layer with a size of $20 \times 20 \times 5$ mm^3. The lowermost layer is a serpentine-structured FPCB with a thickness of 0.1 mm, containing a piece of bare copper with a size of 20×20 mm^2 as an electrode for the PCE-TENG. The porous CB/Ecoflex is securely attached to the Cu electrode by double-sided PI tape. Additionally, the FPCB was designed as a serpentine structure to make it more flexible, to enable placing the PCE-TENG in positions that require monitoring. The failure strain of the entire serpentine interconnection is about 450% (Figure S3, Supplementary Materials). Figure 2c elucidates the working principles of the PCE-TENG, which could be interpreted as a coupling between contact electrification and electrostatic induction. When the Cu electrode is grounded, the PCE-

TENG operates in single-electrode mode, which renders the PCE-TENG well-suited for serving as a pressure sensor to monitor the possible collision around artifacts. During contact electrification, charge transfer occurs at the contact interface between the PI film and the porous CB/Ecoflex. When the PI film makes full contact with the porous CB/Ecoflex, positive charges transfer to the surface of the PI film, while equivalent negative charges transfer to the surface of the porous CB/Ecoflex, due to their different electron-withdrawing abilities (Figure 2c(i)). Upon separation of the materials, positive charges are generated on the Cu electrode to counterpoise the negative charges on the porous CB/Ecoflex, causing free electrons to flow from the Cu electrode to the ground through an external circuit (Figure 2c(ii)). The electron flow persists until the Cu electrode accumulates an equivalent amount of induced charges to that present on the porous CB/Ecoflex, when the PI film and the porous CB/Ecoflex are fully separated (Figure 2c(iii)). When the positively charged PI film nears the porous CB/Ecoflex, the induced positive charges on the Cu electrode diminish, causing a transfer of free electrons from the ground to the Cu electrode until the PI film and the porous CB/Ecoflex make contact (Figure 2c(iv)). Consequently, by repeatedly engaging and disengaging the PI film with the porous CB/Ecoflex, the generation of alternating current signals is achieved. The working principle was further validated through simulation, using the method of finite element analysis implemented in COMSOL Multiphysics, as depicted in Figure S4 (Supplementary Materials).

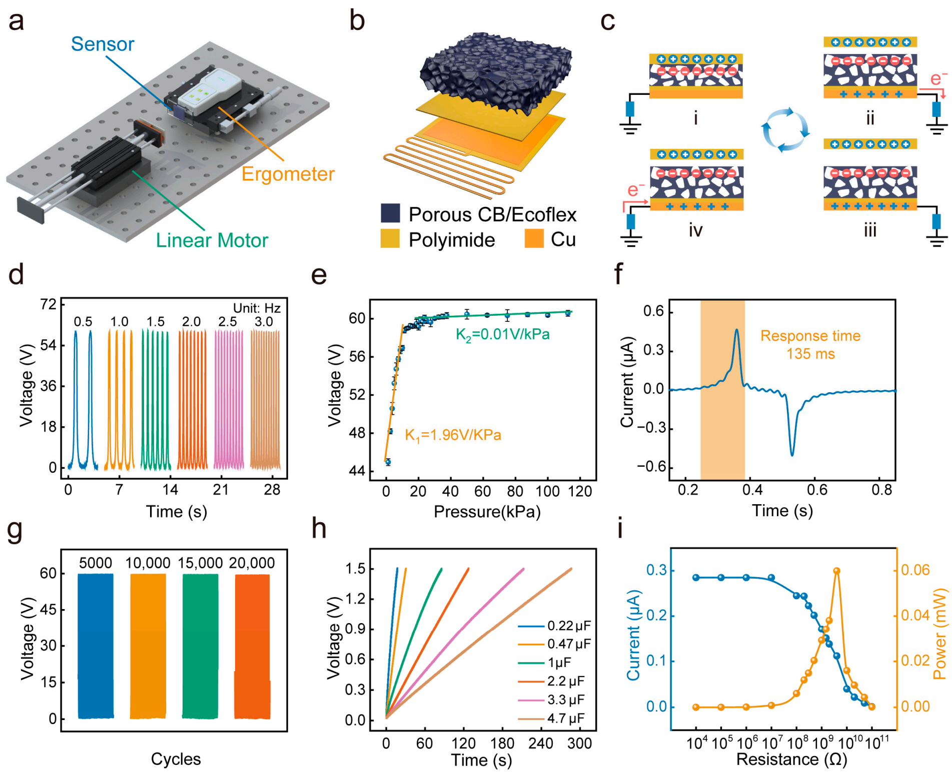

Figure 2. The fundamental electrical output characteristics of the PCE-TENG. (**a**) A 3D schematic diagram of the test platform, (**b**) the PCE-TENG working in a single-electrode mode, and (**c**) its working principles. The open-circuit voltage of the PCE-TENG was acquired (**d**) at 0.5–3.0 Hz, (**e**) under different pressures, and (**g**) under cyclic excitations of 20 N and 3 Hz with good stability over 20,000 cycles. (**f**) The response time of the PCE-TENG. (**h**) The charging curves of different capacitors charged by the PCE-TENG. (**i**) The current and maximum output power curves for the PCE-TENG used as a power supply with different external load resistances (ranging from 10^4 to 10^{11} Ω).

The electrical characteristics of the PCE-TENG are crucial for artifact collision monitoring. The fundamental electrical output characteristics of the PCE-TENG ($20 \times 20 \times 5$ mm^3) with a 2 wt% CB content in the porous CB/Ecoflex (made by mixing CAM and Ecoflex in a weight ratio of 2:1) were evaluated. The open-circuit voltage (V_{oc}), the short-circuit current (I_{sc}), and the short-circuit transferred charge (Q_{sc}) at different frequencies (0.5–3.0 Hz) with an external force of 20 N are shown in Figure 2d and Figure S5 (Supplementary Materials). Notably, V_{oc} and Q_{sc} exhibited minimal variation across different frequencies, whereas I_{sc} demonstrated an increase with increasing frequency. In later applications, the voltage signal is mainly acquired, so the stability of the voltage at different frequencies is incredibly important. To assess the impact of pressure sensitivity, the V_{oc} value of the PCE-TENG was measured across a range of pressures, spanning from 0 Pa to 112 kPa. The relationship between the pressure and V_{oc} is depicted in Figure 2e. The pressure sensitivity is reproducible with small errors after several measurements. According to the fitting analysis, the pressure–voltage curves are divided into two pressure regions of 0.5–15 kPa and 15–112 kPa. The first region has a pressure sensitivity of 1.96 $V \cdot kPa^{-1}$; the second region has a pressure sensitivity of 0.01 $V \cdot kPa^{-1}$. The voltage response to increasing pressure is more pronounced in the pressure region of 0.5–15 kPa compared to that in the region of 15–112 kPa. Additionally, Figure 2f demonstrates that the PCE-TENG possesses a quick response time of 135 ms, highlighting its exceptional ability to promptly detect collision events. Moreover, Figure 2g shows that even after undergoing 20,000 cycles of repetitive operation at 2 Hz and an applied force of 20 N, the output voltage of the PCE-TENG remains largely unchanged. This outcome indicates the remarkable durability and stability of the sensor. The charging capability of the PCE-TENG is depicted in Figure 2h. Notably, the PCE-TENG can charge a 1 μF capacitor to 1.5 V within a duration of 85 s under applied force of 20 N at 2 Hz. Figure 2i illustrates the plots of current and power corresponding to different external load resistances. The output power of the PCE-TENG was calculated using the equation $P = I(t)^2R$, where R represents the load resistance and I(t) denotes the instantaneous current flowing through the resistance. With an external resistance of 4 GΩ, the PCE-TENG achieves a maximum output power of 0.06 mW, suggesting an internal resistance of approximately 4 GΩ. Additionally, Video S1 (Supplementary Materials) presents the potential of the PCE-TENG as a power source capable of illuminating 30 LEDs by applying a force of 20 N at 2 Hz.

These output characteristics enable the use of the PCE-TENG as a self-powered pressure sensor in the SAMS, enabling timely, sensitive, and stable monitoring of small forces on artifacts over long periods of time.

3.3. Optimization of the PCE-TENG

The optimization of the electrical output of the PCE-TENG begins with the influence of the CB content. The use of CB as a doping agent in the contact layer of TENGs has been demonstrated to effectively enhance their electrical output performance, owing to CB's capacity for charge storage [38,39]. We fabricated a total of six types of porous Ecoflex TENGs (made by mixing CAM and Ecoflex in a weight ratio of 2:1) with different CB contents from 1 to 10 wt%. The TENG made with porous pure Ecoflex was utilized as a control. The I_{sc}, V_{oc}, and Q_{sc} values of the porous Ecoflex TENGs with different CB powder contents, under a frequency of 1 Hz and an applied force of 20 N, are illustrated in Figure 3a–c, respectively. As the CB content rises from 0 to 2 wt%, there is an increase in the electrical output. However, beyond 2 wt%, the electrical output begins to decline. This decrease can be attributed to the agglomeration of CB particles, forming bundles that create a leakage current path within the contact layer, as explained in the literature [40]. As shown in Figure 3g, with an increased CB powder content exceeding 2 wt%, the gradual formation of carbon bundles occurs on the surface. The presence of excessive carbon black particles leads to the generation of leakage currents, which, in turn, reduces the quantity of charge on the contact layer. Consequently, the induced charges on the conductive layer are also diminished, resulting in a decrease in electrical output (Figure S6, Supplementary Materials). Thus, a CB content of 2 wt% was chosen as the optimized level.

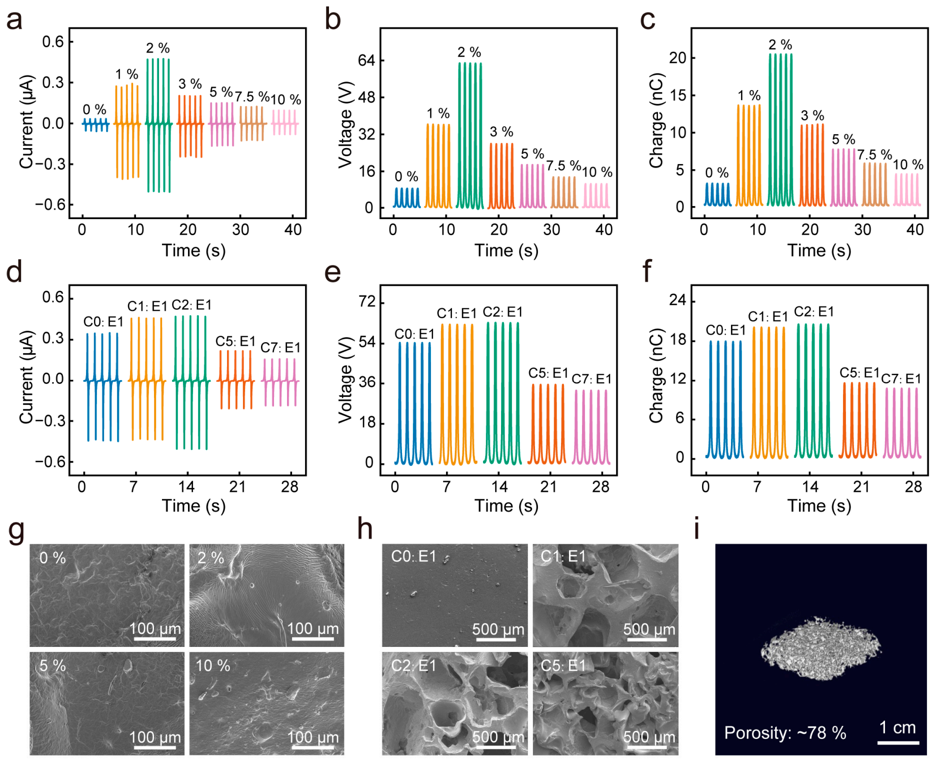

Figure 3. The effects of different contents of CB powder and mixing ratios of CAM and Ecoflex on the electrical output of the TENGs. (**a**) The short-circuit current, (**b**) the open-circuit voltage, and (**c**) the short-circuit transferred charge of the TENGs at a CAM/Ecoflex weight ratio of 2:1 with different carbon black powder contents under applied force of 20 N. Given the optimal CB powder content of 2 wt%, the TENGs were further improved regarding (**d**) the short-circuit current, (**e**) the open-circuit voltage, and (**f**) the short-circuit transferred charge with different mixing ratios of CAM and Ecoflex under applied force of 20 N. (**g**) SEM images of Ecoflex with carbon black powder contents of 0 wt%, 2 wt%, 5 wt%, and 10 wt%. (**h**) The morphology of the solid Ecoflex and the porous CB/Ecoflex with different CAM ratios in micro-scale was visualized through SEM. (**i**) Micro-CT image for the overall view of the porous CB/Ecoflex (made by mixing CAM and Ecoflex in a weight ratio of 2:1, with a 2 wt% CB powder content, porosity~78%).

The surface structure of the contact layer is another influential factor that significantly impacts the electrical output of the PCE-TENG. It has a great influence on the surface charge density, which has a critical role in determining the electrical output performance of the PCE-TENG [41]. Fortunately, it can be easily regulated by adjusting the mixing ratios of CAM and Ecoflex. Consequently, we investigated the impact of the various mixing ratios of CAM and Ecoflex on the electrical output. The samples were distinguished based on the weight ratio of CAM and Ecoflex, denoted by numbers following the letters "C" and "E". For example, C 0:E 1 means pure CB/Ecoflex, and C 1:E 1 means porous CB/Ecoflex made by mixing CAM and Ecoflex in a weight ratio of 1:1. The I_{sc}, V_{oc}, and Q_{sc} values of TENGs with a 2 wt% CB powder content made with different mixing ratios of CAM and Ecoflex are shown in Figure 3d–f, respectively. The porosity of the contact surface continuously increased with an increase in the ratio of CAM to Ecoflex from C 0:E 1 to C 2:E 1, as presented in Figure 3h. The surface charge density also increased with increasing effective contact area, resulting in an elevated electrical output. However, the porous CB/Ecoflex samples made by mixing CAM and Ecoflex in a weight ratio greater than 5:1 had apparently shrunk, lacking mechanical robustness due to their over-large porosity (Figure S7, Supplementary Materials). Repeated loading caused the collapse of these structures, resulting in a reduction in the electrical output due to the decrease in the effective contact area. Therefore, the PCE-TENG made from porous CB/Ecoflex with a 2 wt% CB powder content and with CAM and Ecoflex mixed in a weight ratio of 2:1 achieved the highest electrical output in our experiments. Micro-computed tomography (micro-CT) analysis verified that the porosity of the contact layer reached approximately 78%, as illustrated in Figure 3i. The following formula can be used to calculate the porosity (θ): $\theta = (1 - M/V\rho) \times 100\%$, where M and V are the mass and the volume of an optimized porous CB/Ecoflex sample, respectively, and ρ is the density of a control sample of the same volume but without a porous structure. The calculated porosity was 78%.

3.4. Mechanical Properties

A porous structure is ideal for vibration absorption, which is important for protecting artifacts from damage during transportation. We further evaluated the vibration absorption ability of the porous CB/Ecoflex, as compared with the CB/Ecoflex, pure Ecoflex, and porous pure Ecoflex, through their rebound rates and compressive properties. A falling ball tester was used to evaluate their vibration absorption ability during an impact (Figure 4a). A 100 g ball was released from a height of 25 cm in free-fall state, and the height it bounced up after impacting on the sample under test was recorded by a high-speed camera, as shown in Figure 4b. By calculating the average rebound rate, we can characterize the cushioning effect of the sample. The averaged rebound rates of the four materials are depicted in Figure 4d. The porous CB/Ecoflex and the porous pure Ecoflex showed higher cushioning performance. Figure 4c displays the stress–strain relationships under compression of the four materials. The compressibility of the porous samples was significantly improved compared to that of the samples without pores, due to the low elastic modulus of the porous samples. These results suggest that the porous structure contributes to the improvement of mechanical vibration absorption.

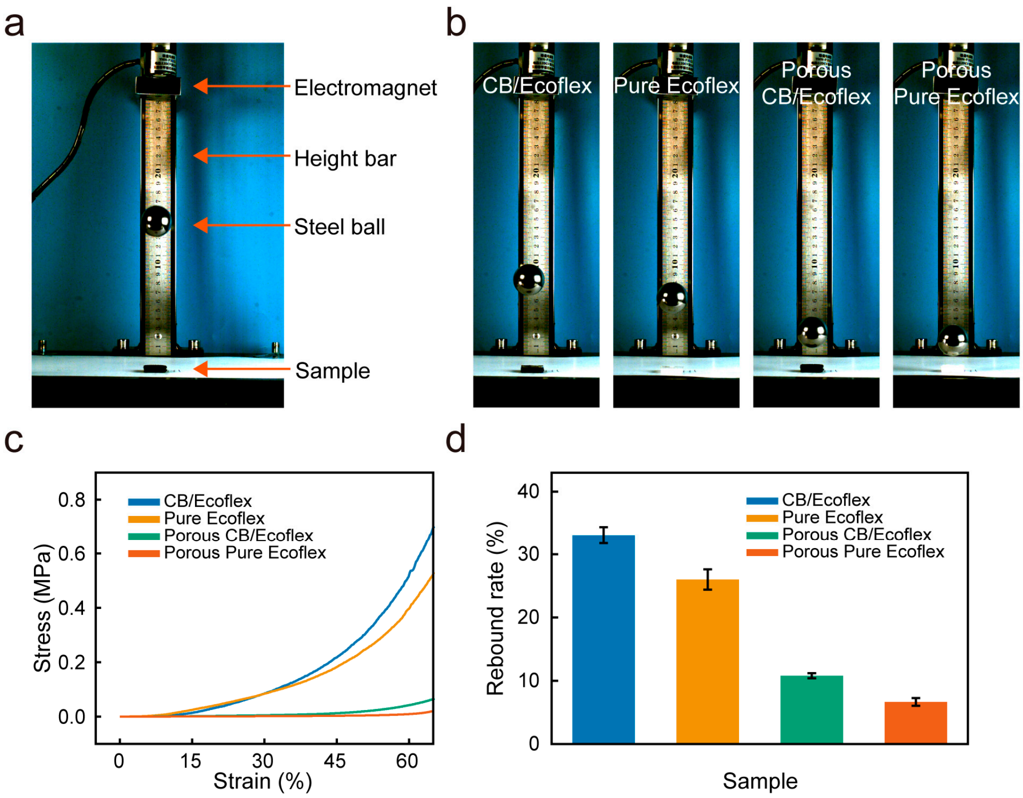

Figure 4. The cushioning performance of the CB/Ecoflex, pure Ecoflex, porous CB/Ecoflex, and porous pure Ecoflex. (**a**) Photograph of a falling ball tester. (**b**) Photographs of a falling ball hitting a sample and bouncing to its maximum height were taken by a high-speed camera for different samples. (**c**) The stress–strain relationships under compression of CB/Ecoflex, pure Ecoflex, porous CB/Ecoflex, and porous pure Ecoflex, with their rebound rates shown in (**d**).

Due to the mechanical properties of the porous CB/Ecoflex, the porous structure can provide additional elastic deformation space in the event of a collision, absorbing and dispersing kinetic energy, and can therefore be used as a protective material in the transportation of artifacts.

3.5. Application of the PCE-TENG in the SAMS

Due to its self-powered sensing and cushioning performance, the PCE-TENG has great application potential in collision monitoring, especially for artifact transportation. We constructed a SAMS using six PCE-TENGs as self-powered pressure sensors in combination with integrated circuits and a monitoring terminal. The integrated circuit encompasses a pre-amplifier, a multi-channel analog-to-digital (AD) conversion module, a microprocessor unit (STM32), and a Wi-Fi module (ESP32) for signal acquisition and processing. The pre-amplifier amplifies the signal, which is subsequently digitized by the AD chip; under the control of the microprocessor, the signal is then transmitted to the monitoring terminal via the Wi-Fi module. The monitoring terminal, employing six simultaneous sampling channels with a sampling rate of 2 K/s each, utilizes a LabVIEW computer program for signal reception, display, and storage. For a comprehensive depiction of the circuit diagram, please refer to Figure S1 (Supplementary Materials). We used a practical case of a porcelain vase to demonstrate a collision-sensing situation. A flow chart of the working principle of the SAMS is shown in Figure 5a. When the porcelain vase tilts during the simulated transportation process, it touches the PCE-TENG and enables the conversion of mechanical energy into electrical signals. The integrated circuit board collects the signals generated by the PCE-TENG in real time and transmits them to the monitoring terminal via a Wi-Fi communication module. If the collision level surpasses the pre-determined threshold, the monitoring terminal's user interface promptly presents real-time collision alarms along with precise direction information. The triggered alarm will continuously alert the carriers until effective measures are taken to return the artifact to its normal posture, and then the alarm will be dismissed. Thus, the truck carrier or worker could lower their speed or tighten their behavior to better protect the artifacts. The setup of a porcelain vase transport package equipped with a SAMS is photographed in Figure 5b. Figure 5c displays the six PCE-TENGs with the stretchable six-way electrode FPCB, capable of simultaneously monitoring collisions occurring in six directions: front, behind, left, right, up, and down. The inset image shows the integrated acquisition circuit board. The user interface of the SAMS was programmed using LabVIEW to consist of each channel's real-time voltage signal area and an alarm display area (Figure 5d). Figure 5e exhibits the output results at different pressures obtained by wireless acquisition. The experimental results demonstrate that the output voltage of the PCE-TENG exhibits a progressive increase with the continuous application of pressure, indicating the significant potential of the PCE-TENG for different collision-monitoring applications.

Video S2 (Supplementary Materials) further demonstrates the ability of the real-time direction alarm during a simulated process of manual transportation of the porcelain vase transport package equipped with a SAMS; this forms the basis for achieving smart artifact transportation monitoring. The visualization of collision alarms in different directions is achieved by analyzing and calculating the real-time voltage signals using algorithms such as peak detection and threshold judgment in the LabVIEW software. Figure 5f illustrates the alarm mechanism based on the voltage signal for triggering and dismissing the alarm. Taking the right-side alarm situation as an example, when the porcelain vase impacts the right-side PCE-TENG, it generates a trough signal; subsequently, the right-side alarm light is triggered and remains on constantly, reminding carriers to adopt the corresponding action continuously. The alarm is dismissed when the porcelain vase is back to its normal position. It is tremendously important to send real-time alarms and alert carriers of the specific orientation of collision when a collision happens; this help carriers to correct inappropriate transportation methods in a timely manner to better protect the safety of artifacts.

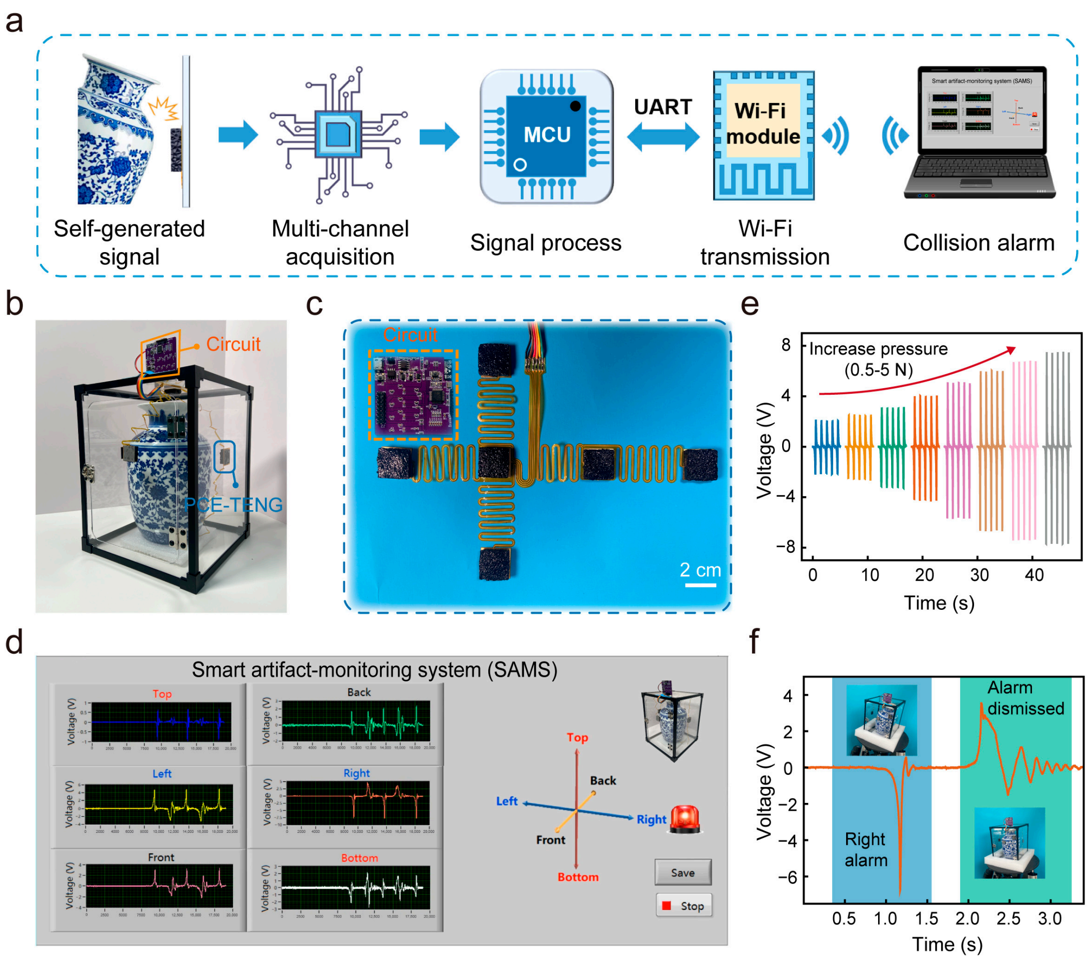

Figure 5. Application of PCE-TENGs in the SAMS. (**a**) A flow chart of the working principle of the SAMS. (**b**) Photograph of PCE-TENGs on the front, back, left, right, up, and down sides for wireless collision monitoring, taking a porcelain vase as an example. (**c**) Photographs of the PCE-TENGs with a stretchable 6-way electrode FPCB and the integrated circuit board with functions of multi-channel signal acquisition, processing, and Wi-Fi transmission. (**d**) The screenshot shows the SAMS user interface. (**e**) Output voltage signals from the wireless monitoring system under different pressures. (**f**) The alarm mechanism of the SAMS based on the output voltage for triggering and dismissing the alarm.

In summary, we developed a SAMS with functions of Wi-Fi transmission (which avoids complicated wiring), multi-directional collision monitoring, and artifact transport safety posture confirmation, which can better meet the needs of the actual process of artifact transportation monitoring.

4. Conclusions

The monitoring of artifacts during transportation is crucial to the protection of cultural relics from damage during cultural exchanges. However, current collision detection techniques have limitations regarding power supply deficiencies, buffer protection benefits, and real-time monitoring. In this work, we presented an approach for self-powered sensing in a smart artifact-monitoring system (SAMS) using porous carbon black (CB)/Ecoflex triboelectric nanogenerators (PCE-TENGs). The key advances in our SAMS include the following: (1) PCE-TENGs were assembled using a porous Ecoflex layer embedded with CB powder and a flexible printed circuit board (FPCB), which enabled cushioning, stretchability, pressure sensitivity, and durability. Our results demonstrate a rebound rate of about 10%, a low compression modulus, and pressure sensitivity of 1.96 V·kPa^{-1} (<15 kPa). This design allows for the simultaneous implementation of cushioning and sensing functions.

(2) The influence of the CB doping content in the contact material and its surface structure on the electrical output was investigated; excess carbon black and high porosity were found to have a negative impact on the electrical output. This provides guidance for the design of contact materials. (3) To monitor collisions during artifact transportation in real time, we placed six PCE-TENGs on the six inner faces of an artifact transport package and connected them to a multi-channel wireless acquisition circuit board. Real-time collision alarms with direction information were transmitted to the monitoring terminal via Wi-Fi. Additionally, a visual alarm mechanism was constructed to assist artifact carriers in confirming the safe transport status of artifacts. This work provides a promising strategy for artifact transportation monitoring and has essential implications for package optimization, intelligent logistics, and self-powered wireless sensing.

Supplementary Materials: The following supporting information can be downloaded at: https://www.mdpi.com/article/10.3390/electronics12143031/s1, Figure S1. Detailed circuit schematic of the SAMS; Figure S2. Compression recovery property of the porous CB/Ecoflex; Figure S3. Photograph of the serpentine interconnecting FPCB under mechanical stretching with various strains. Simulation results of uniaxial stretching of the whole serpentine interconnecting FPCB at 0.1 N; Figure S4. The spatial distribution of the electric field at different stages; Figure S5. The I_{sc} and Q_{sc} values of a PCE-TENG (made by mixing CAM and Ecoflex in a weight ratio of 2:1, with a 2 wt% CB powder content) at various applied frequencies (0.5–3.0 Hz); Figure S6. Schematic of the dynamic behavior of electrical charge in PCE-TENGs with low CB content and high CB content; Figure S7. Photographs of original samples and porous CE/Ecoflex washed with ethanol; Video S1. Lighting up 30 LEDs using a PCE-TENG; Video S2. Demonstration of the real-time direction alarm for a porcelain vase transport package equipped with a SAMS during a simulated manual transportation process.

Author Contributions: Conceptualization, J.Z., D.L. and Z.L.W.; Methodology, J.Z., E.S., C.L., S.X., W.T., L.N.Y.C. and D.L.; Software, C.L.; Validation, J.Z., E.S., C.L. and S.X.; Formal analysis, J.Z. and D.L.; Investigation, J.Z., W.T., L.N.Y.C. and D.L.; Resources, Z.L.W.; Data curation, J.Z., E.S. and C.L.; Writing—original draft, J.Z. and D.L.; Writing—review and editing, D.L. and Z.L.W.; Visualization, C.L.; Supervision, D.L. and Z.L.W.; Project administration, D.L. and Z.L.W.; Funding acquisition, Z.L.W. All authors have read and agreed to the published version of the manuscript.

Funding: This research was funded by the National Key R&D Project from the Ministry of Science and Technology of the People's Republic of China (2021YFA1201601) and the National Natural Science Foundation of China (Grant Nos. 52002028, 52192610).

Data Availability Statement: The data presented in this study are available on reasonable request from the corresponding author.

Conflicts of Interest: The authors declare no conflict of interest.

References

1. Bae, C.J.; Douka, K.; Petraglia, M.D. On the origin of modern humans: Asian perspectives. *Science* **2017**, *358*, eaai9067. [CrossRef] [PubMed]
2. Ardelean, C.F.; Becerra-Valdivia, L.; Pedersen, M.W.; Schwenninger, J.L.; Oviatt, C.G.; Macias-Quintero, J.I.; Arroyo-Cabrales, J.; Sikora, M.; Ocampo-Diaz, Y.Z.E.; Rubio, C., II; et al. Evidence of human occupation in Mexico around the Last Glacial Maximum. *Nature* **2020**, *584*, 87–92. [CrossRef] [PubMed]
3. Inomata, T.; Triadan, D.; Vazquez Lopez, V.A.; Fernandez-Diaz, J.C.; Omori, T.; Mendez Bauer, M.B.; Garcia Hernandez, M.; Beach, T.; Cagnato, C.; Aoyama, K.; et al. Monumental architecture at Aguada Fenix and the rise of Maya civilization. *Nature* **2020**, *582*, 530–533. [CrossRef] [PubMed]
4. Zhang, J.; Guo, M.; Li, B.; Lu, R. A transport monitoring system for cultural relics protection based on blockchain and internet of things. *J. Cult. Herit.* **2021**, *50*, 106–114. [CrossRef]
5. Kamba, N.; Wada, H.; Tsukada, M.; Takagi, Y.; Imakita, K. Measurement and Analysis of the Global Transport Environment for Packing Cases for Artifacts. *Stud. Conserv.* **2013**, *53*, 60–63. [CrossRef]
6. Sánchez-Belenguer, C.; Vendrell-Vidal, E.; Sánchez-López, M.; Díaz-Marín, C.; Aura-Castro, E. Automatic Production of Tailored Packaging for Fragile Archaeological Artifacts. *J. Comput. Cult. Herit.* **2015**, *8*, 1–11. [CrossRef]
7. Saunders, D. Monitoring shock and vibration during the transportation of paintings. *Natl. Gallery Tech. Bull.* **1998**, *19*, 64–73.
8. Saunders, D.; Sitwell, C.L.; Staniforth, S. Soft Pack-The Soft Option? In *Art in Transit: Studies in the Transport of Paintings*; Mecklenburg, M.F., Ed.; National Gallery of Art: Washington, DC, USA, 1991; pp. 311–321.

9. Lasyk, Ł.; Łukomski, M.; Bratasz, Ł.; Kozłowski, R. Vibration as a Hazard during the Transportation of Canvas Paintings. *Stud. Conserv.* **2013**, *53*, 64–68. [CrossRef]
10. Rouillard, V.; Lamb, M.J. On The Performance of Mechanical Shock Indicators. *Packag. Technol. Sci.* **2017**, *30*, 257–268. [CrossRef]
11. Proto, S.; Di Corso, E.; Apiletti, D.; Cagliero, L.; Cerquitelli, T.; Malnati, G.; Mazzucchi, D. REDTag: A Predictive Maintenance Framework for Parcel Delivery Services. *IEEE Access* **2020**, *8*, 14953–14964. [CrossRef]
12. Mehamud, I.; Marklund, P.; Bjorling, M.; Shi, Y.J. Machine condition monitoring enabled by broad range vibration frequency detecting triboelectric nano-generator (TENG)-based vibration sensors. *Nano Energy* **2022**, *98*, 107292. [CrossRef]
13. Zhang, X.; Zhao, J.; Fu, X.; Lin, Y.; Qi, Y.; Zhou, H.; Zhang, C. Broadband vibration energy powered autonomous wireless frequency monitoring system based on triboelectric nanogenerators. *Nano Energy* **2022**, *98*, 107209. [CrossRef]
14. Chen, J.; Wang, Z.L. Reviving Vibration Energy Harvesting and Self-Powered Sensing by a Triboelectric Nanogenerator. *Joule* **2017**, *1*, 480–521. [CrossRef]
15. Haroun, A.; Tarek, M.; Mosleh, M.; Ismail, F. Recent Progress on Triboelectric Nanogenerators for Vibration Energy Harvesting and Vibration Sensing. *Nanomaterials* **2022**, *12*, 2960. [CrossRef] [PubMed]
16. Yuan, M.; Yu, W.; Jiang, Y.; Ding, Z.; Zhang, Z.; Zhang, X.; Xie, Y. Triboelectric nanogenerator metamaterials for joint structural vibration mitigation and self-powered structure monitoring. *Nano Energy* **2022**, *103*, 107773. [CrossRef]
17. Liu, C.; Wang, Y.; Zhang, N.; Yang, X.; Wang, Z.; Zhao, L.; Yang, W.; Dong, L.; Che, L.; Wang, G.; et al. A self-powered and high sensitivity acceleration sensor with V-Q-a model based on triboelectric nanogenerators (TENGs). *Nano Energy* **2020**, *67*, 104228. [CrossRef]
18. Mu, J.; Han, X.; Yu, J.; Song, J.; He, J.; Geng, W.; Zou, J.; Xian, S.; Chou, X. Magnetic Levitation Type Double Helix Self-Powered Acceleration Sensor Based on ZnO-RTV Film. *Adv. Mater. Technol.* **2021**, *7*, 2100802. [CrossRef]
19. Zhang, B.; Wu, Z.; Lin, Z.; Guo, H.; Chun, F.; Yang, W.; Wang, Z.L. All-in-one 3D acceleration sensor based on coded liquid–metal triboelectric nanogenerator for vehicle restraint system. *Mater. Today* **2021**, *43*, 37–44. [CrossRef]
20. Qi, Y.; Kuang, Y.; Liu, Y.; Liu, G.; Zeng, J.; Zhao, J.; Wang, L.; Zhu, M.; Zhang, C. Kirigami-inspired triboelectric nanogenerator as ultra-wide-band vibrational energy harvester and self-powered acceleration sensor. *Appl. Energy* **2022**, *327*, 120092. [CrossRef]
21. Wang, Z.; Yu, Y.; Wang, Y.; Lu, X.; Cheng, T.; Bao, G.; Wang, Z.L. Magnetic Flap-Type Difunctional Sensor for Detecting Pneumatic Flow and Liquid Level Based on Triboelectric Nanogenerator. *ACS Nano* **2020**, *14*, 5981–5987. [CrossRef]
22. Song, Z.; Zhang, X.; Wang, Z.; Ren, T.; Long, W.; Cheng, T.; Wang, Z.L. Nonintrusion Monitoring of Droplet Motion State via Liquid-Solid Contact Electrification. *ACS Nano* **2021**, *15*, 18557–18565. [CrossRef] [PubMed]
23. Cao, L.N.Y.; Xu, Z.; Wang, Z.L. Application of Triboelectric Nanogenerator in Fluid Dynamics Sensing: Past and Future. *Nanomaterials* **2022**, *12*, 3216. [CrossRef] [PubMed]
24. Kim, W.; Choi, D.; Kwon, J.Y.; Choi, D. A self-powered triboelectric microfluidic system for liquid sensing. *J. Mater. Chem. A* **2018**, *6*, 14069–14076. [CrossRef]
25. Lei, Y.; Yang, J.; Xiong, Y.; Wu, S.; Guo, W.; Liu, G.-S.; Sun, Q.; Wang, Z.L. Surface engineering AgNW transparent conductive films for triboelectric nanogenerator and self-powered pressure sensor. *Chem. Eng. J.* **2023**, *462*, 142170. [CrossRef]
26. Ke, K.H.; Chung, C.K. High-Performance Al/PDMS TENG with Novel Complex Morphology of Two-Height Microneedles Array for High-Sensitivity Force-Sensor and Self-Powered Application. *Small* **2020**, *16*, e2001209. [CrossRef]
27. Lee, S.; Park, J.W. Fingerprint-inspired triboelectric nanogenerator with a geometrically asymmetric electrode design for a self-powered dynamic pressure sensor. *Nano Energy* **2022**, *101*, 107546. [CrossRef]
28. Rana, S.M.S.; Rahman, M.T.; Salauddin, M.; Sharma, S.; Maharjan, P.; Bhatta, T.; Cho, H.; Park, C.; Park, J.Y. Electrospun PVDF-TrFE/MXene Nanofiber Mat-Based Triboelectric Nanogenerator for Smart Home Appliances. *ACS Appl. Mater. Interfaces* **2021**, *13*, 4955–4967. [CrossRef]
29. Fan, F.R.; Tian, Z.Q.; Wang, Z.L. Flexible triboelectric generator! *Nano Energy* **2012**, *1*, 328–334. [CrossRef]
30. Su, E.; Li, H.; Zhang, J.; Xu, Z.; Chen, B.; Cao, L.N.Y.; Wang, Z.L. Rationally Designed Anti-Glare Panel Arrays as Highway Wind Energy Harvester. *Adv. Funct. Mater.* **2023**, *33*, 2214934. [CrossRef]
31. Deng, Z.; Xu, L.; Qin, H.; Li, X.; Duan, J.; Hou, B.; Wang, Z.L. Rationally Structured Triboelectric Nanogenerator Arrays for Harvesting Water-Current Energy and Self-Powered Sensing. *Adv. Mater.* **2022**, *34*, e2205064. [CrossRef]
32. Guan, Q.; Lu, X.; Chen, Y.; Zhang, H.; Zheng, Y.; Neisiany, R.E.; You, Z. High-Performance Liquid Crystalline Polymer for Intrinsic Fire-Resistant and Flexible Triboelectric Nanogenerators. *Adv. Mater.* **2022**, *34*, e2204543. [CrossRef] [PubMed]
33. Heo, D.; Kim, T.; Yong, H.; Yoo, K.T.; Lee, S. Sustainable oscillating triboelectric nanogenerator as omnidirectional self-powered impact sensor. *Nano Energy* **2018**, *50*, 1–8. [CrossRef]
34. Liu, Y.; Li, D.; Hou, Y.; Wang, Z.L. Grating-Structured Freestanding Triboelectric Nanogenerator for Self-Powered Acceleration Sensing in Real Time. *Adv. Mater. Technol.* **2022**, *8*, 2200746. [CrossRef]
35. Kou, H.; Wang, H.; Cheng, R.; Liao, Y.; Shi, X.; Luo, J.; Li, D.; Wang, Z.L. Smart Pillow Based on Flexible and Breathable Triboelectric Nanogenerator Arrays for Head Movement Monitoring during Sleep. *ACS Appl. Mater. Interfaces* **2022**, *14*, 23998–24007. [CrossRef]
36. Fan, Y.J.; Meng, X.S.; Li, H.Y.; Kuang, S.Y.; Zhang, L.; Wu, Y.; Wang, Z.L.; Zhu, G. Stretchable Porous Carbon Nanotube-Elastomer Hybrid Nanocomposite for Harvesting Mechanical Energy. *Adv. Mater.* **2017**, *29*, 1603115. [CrossRef] [PubMed]
37. Park, J.; Kim, I.; Yun, J.; Kim, D. Liquid-metal embedded sponge-typed triboelectric nanogenerator for omnidirectionally detectable self-powered motion sensor. *Nano Energy* **2021**, *89*, 106442. [CrossRef]

38. Choi, J.H.; Ra, Y.; Cho, S.; La, M.; Park, S.J.; Choi, D. Electrical charge storage effect in carbon based polymer composite for long-term performance enhancement of the triboelectric nanogenerator. *Compos. Sci. Technol.* **2021**, *207*, 108680. [CrossRef]
39. Zhang, W.; Liu, Q.; Chao, S.; Liu, R.; Cui, X.; Sun, Y.; Ouyang, H.; Li, Z. Ultrathin Stretchable Triboelectric Nanogenerators Improved by Postcharging Electrode Material. *ACS Appl. Mater. Interfaces* **2021**, *13*, 42966–42976. [CrossRef]
40. Kim, J.; Ryu, H.; Lee, J.H.; Khan, U.; Kwak, S.S.; Yoon, H.J.; Kim, S.W. High Permittivity CaCu3Ti4O12 Particle-Induced Internal Polarization Amplification for High Performance Triboelectric Nanogenerators. *Adv. Energy Mater.* **2020**, *10*, 1903524. [CrossRef]
41. Baytekin, H.T.; Patashinski, A.Z.; Branicki, M.; Baytekin, B.; Soh, S.; Grzybowski, B.A. The mosaic of surface charge in contact electrification. *Science* **2011**, *333*, 308–312. [CrossRef]